SUPPORTING MATERIAL

ARROW fabrication parameters

layer	1	2	1	2	1	2	**core**	2	1	2	1	2	1
thickness	1,876	100	268	100	268	100	**5,000**	132	286	146	300	128	3,016

Table S1: Thickness of the ARROW layers in nm. Composition: 1 = SiO_2, 2 = SiN. The silicon substrate is below the first layer and the last layer is followed by air.

Optical performance of the ARROW network

To validate the waveguiding properties of the fabricated network we have taken white-light transmission spectra of various waveguide sections. The white-light continuum was generated by femtosecond pulses of 820 nm light launched into a photonic crystal fiber. It was subsequently coupled through a single mode fiber into the end facet of the waveguide. The normalized transmission shown in Fig. S1 was obtained for two distinct polarizations. Calibration points for the related waveguide loss at 532 and 820 nm were obtained as described in Ref. S1 and in the main text. These numbers are meant as a guide to the eye, since the loss coefficients were determined for the liquid core only, while the transmission also includes a portion of solid core. It can nevertheless be seen, that the ARROW waveguides provide a broad low-loss transmission window extending from 500 to 900 nm and are thus well suited for a wide class of optical analysis methods

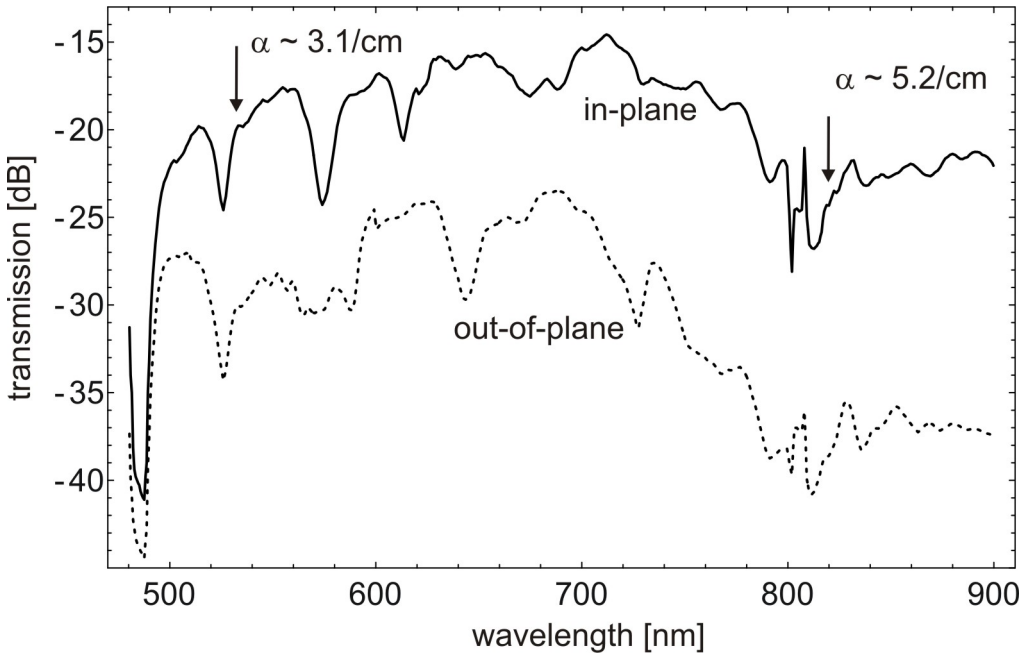

Figure S1. Spectral transmission of a waveguide section consisting of 3.6 mm liquid core merging into 5.5 mm solid core. Solid line: polarization in plane of the chip, broken line: polarization out of plan of the chip. The arrow indicates the wavelength at which the loss of the liquid core was determined in another measurement.

Characterization of the LB trap

The performance parameters of the trap where obtained in two different ways. In the first method a histogram of the fluctuating particle location due to Brownian thermal aggitation is built from a video recording. The extended duration of the measurement makes it also sensitive to external influences like instabilties of the trapping powers and pressure drift that are introduced through the non-integrated optical components used in this investigation. The presence of such slow disturbances can also be read from the analysis of the fluctuation power spectrum. As a result, the time-averaged trapping

potential appears weaker than the instantaneous potential. A measurement of the latter is attempted using a relaxation method. The particle is deliberately aggitated by switching one trapping beam temporarily off. When the trap is re-engaged the particle relaxes to the original trapping point within a few seconds. The result of this measurement describes the properties of an optimized trap in which technical deviations are overcome, e.g. by complete integration. The procedures are now described in more detail.

Under the influence of the two trapping beams, the particle follows a trajectory of the form: $z(t) = -\frac{1}{\alpha}\mathrm{Log}\left(\frac{1+\mathrm{Exp}(-ht+\alpha k)}{1-\mathrm{Exp}(-ht+\alpha k)}\right)$ (h and k are constants) as shown in Fig. S2.

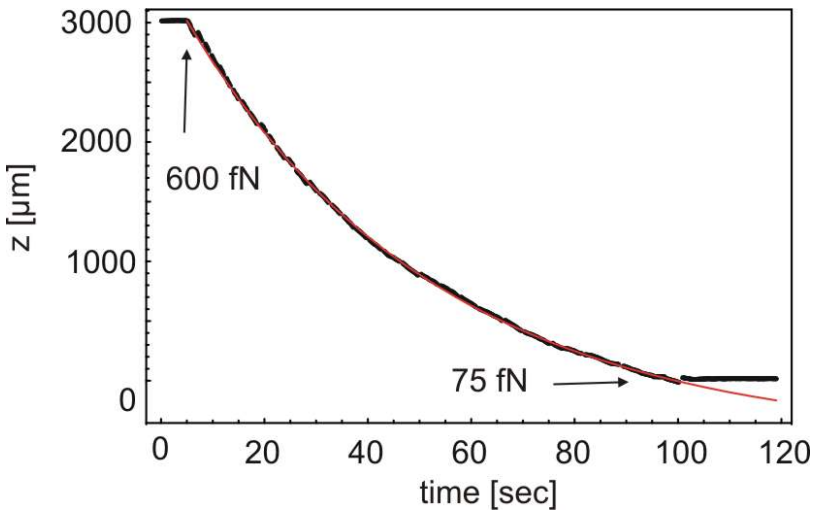

Figure S2. Trajectory of a 1µm PS particle falling into a loss-based dual-beam trap. Trapping beams: 2 x 300 mW input power at the chip edges at 820 nm.

The bead comes to a standstill at t=100s before reaching the absolute bottom of the trap. This effect is caused by the existence of higher order transverse modes in the trapping beams [S1]. Different transverse wavenumbers $k_{x,y}^{n,m}$ (modes; n, m: mode index)

lead to different propagation constants $k_z^{n,m}$ and subsequently to beating of the modes with periods $\Delta k_z^{nm;n'm'} z = (k_z^{nm} - k_z^{n'm'})z$ [S1]. This causes a spatial variation of the beam intensity I(x, y, z) and hence of the radiation pressure coefficient Q(x, y, z), leading to a modulation of the gradient and scattering forces with position. Nevertheless, intensity gradients in the *z*-direction remain negligible. Therefore, the particle is held on a path *z(t)* determined by the highest intensity in the (*x, y*)-profile along which a longitudinal potential may be defined from the sum of the scattering forces of the trapping beams. Eventually, the modulation of these forces according to the beating patterns produces a local potential landscape that is superimposed on the global loss-induced potential. As can be seen from figure S1, the particle was trapped in such a local potential with an escape force exceeding 75 fN. The mode beating can be minimized by careful waveguide design to reduce coupling into higher order ARROW modes at the chip facets and waveguide junctions.

The characteristic parameters of optical traps can be found from the motion of objects under the influence of thermal [S2] or external forces [S3]. To this end, the particle position was recorded over 8,000 frames (800 seconds), showing constrained Brownian motion (Fig. S3A). A histogram and the probability distribution of the particle locations with a bin width of $\delta x = \delta z = 100$ nm were then created from the trajectory (figure S3B). From the Boltzmann law $p(x,z) = c\,Exp(-U(x,z)/kT)$ (c: normalization factor) we then derive a potential $U(x,z)$ which can be approximated by a two-dimensional parabola $U(x,z) \approx \frac{1}{2}(k_x x^2 + k_z z^2)$ to obtain the effective spring constants as shown in figure S3C and D.

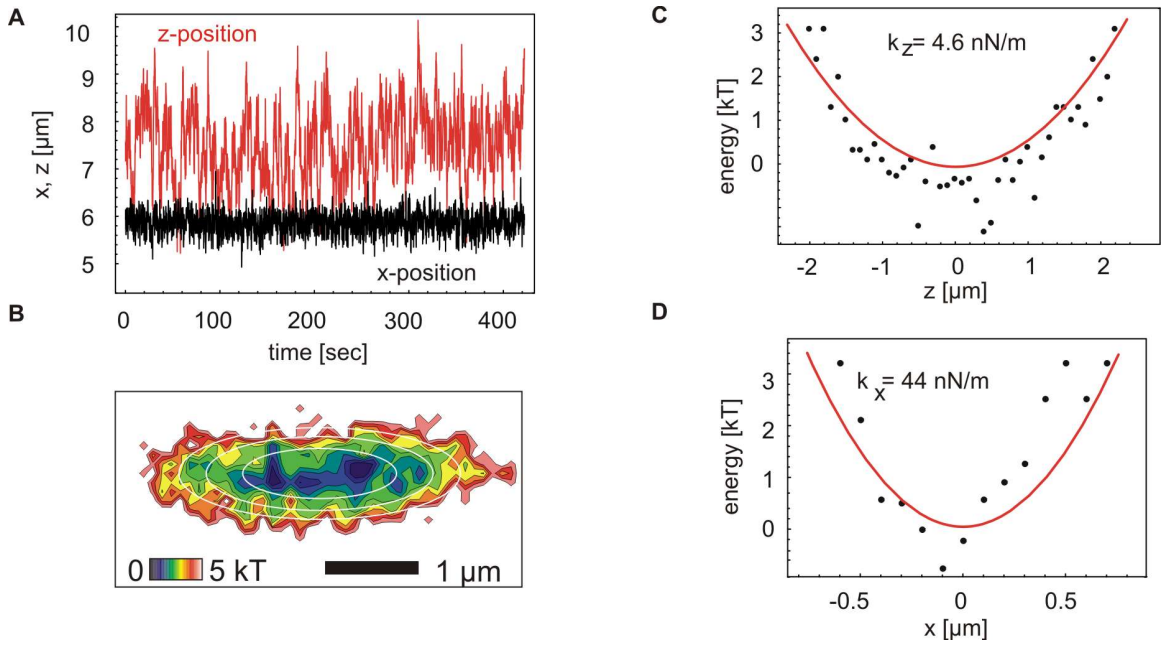

Figure S3. **A**: Fluctuating particle position in a loss-based dual-beam trap. 6 µm mark the waveguide center on the x-scale, while z has an arbitrary offset. **B**: The potential U(*x,z*) derived from the particle locations. No data is available in the white regions of the plot. **C** and **D**: Force constants determined from a two-dimensional parabolic fit to U(*x,z*).

Alternatively, the dual-beam trap lends itself to a relaxation measurement in which one of the trapping beams is temporarily switched off. During the off-time the particle is driven by the sole action of the remaining beam. Since the scattering force from a *single* beam $F_l^{Sca}(\Delta z)$ remains constant over small excursions Δz, the particle moves at constant velocity for 0.5s<t<1s as can be seen in figure S4. When the second beam is unblocked, the particle returns to the trap center under the influence of the linear restoring force $F_{tot}(z) = k_z z$. The corresponding exponential trajectory for t>1s is used to determine the effective spring constant.

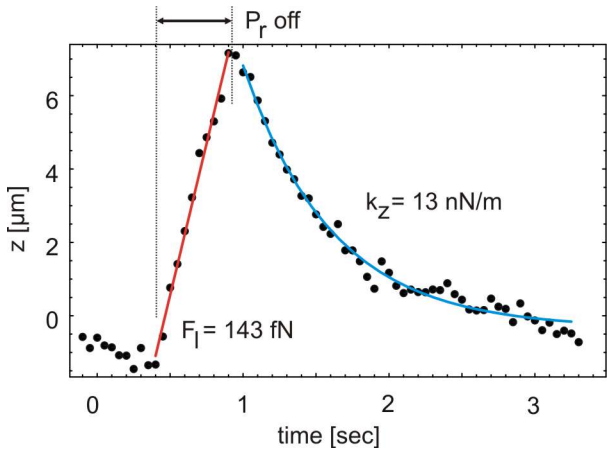

Figure S4. Particle excursion during an intermittent blockage of the right trapping beam, followed by relaxation back to the trapping point.

The noise spectrum of the particle motion was analyzed to identify the cause of the discrepancy between the dynamic and the statistical measurement of k_z. In figure S4A and B we show the power spectral density and the Allan deviation [S4]. This two-sample variance is used to identify noise characteristics by the slope in a double-logarithmic plot for different averaging times, typically but not exclusively for clock oscillators and lasers. Both quantities show nearly free Brownian fluctuations at high frequencies (small averaging times), a decrease in the noise in the intermediate range, and a recurrence of noise in the lowest frequencies. The latter additional noise component has an Allan slope near 0.5 and can be ascribed to a random walk process. We attribute this to fluctuations in the light delivery system which consist of laser to fiber and fiber to fiber coupling stages. These fluctuations result in a fluctuation of the trapping point which is apparent in the particle trajectory. Therefore, we feel confident that the trap stiffness determined by the statistical method underestimates the true value which is reliably determined from the dynamical method. The x-position, on the other hand, is mostly unaffected since the large

power offset given by the sum of the two beams largely reduces the *relative* power fluctuations. Moreover, the fluctuations would not induce directed motion of the particle but only strengthen or weaken of the gradient forces. Obviously, the stability of the trap can be improved if the light sources are directly integrated on the chip in the form of laser diodes.

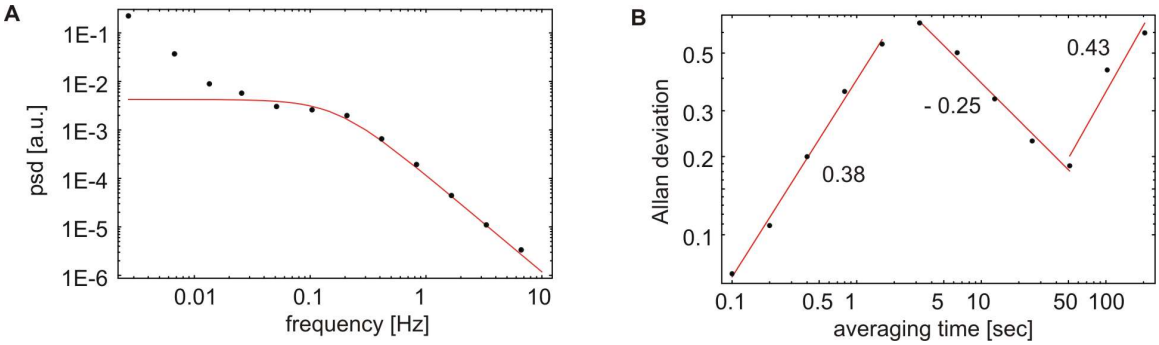

Fig. S5. **A**: Power spectral density (points) with a Lorentzian fit (line). **B**: Allan deviation plot with the linear slopes as indicated. The data used for the calculations are displayed in figure S3A.

Characterization of the DB trap

Divergence based traps formed by counter-propagating beams that emerge from solid-core waveguides intersecting the liquid channel were characterized in a similar manner as the LB-trap. Fig. S6 shows the time-dependent x- and z-positions of a 1 µm latex particle in water that is captured by 2 x 10 mW (measured at the chip input facets) of light at 532 nm. The Brownian motion analysis leads to a trap stiffness of $k_x = 25\,\mathrm{nN/m}$ and $k_z = 32\,\mathrm{nN/m}$, respectively.

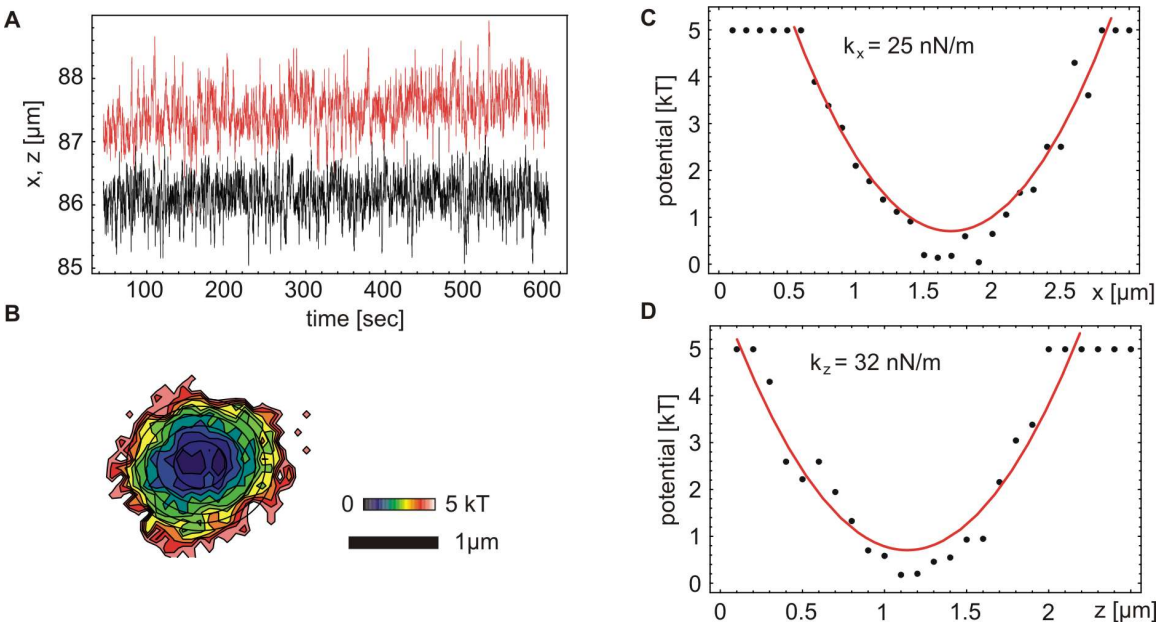

Fig. S6. **A**: X- and z-positions of a latex particle held in a DB intersection trap. **B**: Potential calculated from the probability distribution in **A**. **C** and **D**: Parabolic fits for the trapping potential.

To obtain the Gaussian potential $U(r) = -Q_{grad}\, I_0\, Exp(-2z^2 / w_0^2)$ with Q_{grad}: the gradient force efficiency, I_0: the beam intensity at r = 0 and w_0: the beam waist (at x = 0) from this limited set of sampling points, the trapping force is expanded to first order around the trapping point r=(x,y,z)=(0,0,z): $F = Q_{grad} \nabla I(z) = -Q_{grad}\, I_0\, 4z / w_0^2 + O(3)$. To estimate the unknown coefficients, the force is set equal to the measured linear force $F = k_{eff}\, z$, which leads to a potential depth of $U_0 = I_0\, Q_{grad} = k_{eff} w_0^2 / 4$. For the given parameters of $k_z = 30\, nN/m$ and $w_0 = 3\mu m$ we find $U_0 \approx 6 \cdot 10^{-20}\, J \approx 18\, kT$. The maximum force is reached at the turning point of the Gaussian at $r = \pm w_0 / 2$, where $|F_{\max}| = 2 Q_{grad} I_0 / w_0 \sqrt{e}$ and amounts to $F_{\max} \approx 0.05\text{pN}$ in the present case. We note that the escape force presented in the main body of the paper of $F_{esc} \approx 0.3\,\text{pN}$ was measured

on a differently designed waveguide and corresponds to a potential about six times deeper.

Dual trap potential

Dual traps are frequently used to measure forces and length changes in experiments that investigate the elastic properties of linear macro-molecules or the workings of molecular motors. The linkage between the bead handles via the molecule is sometimes accomplished in-situ to avoid unintended cross-linking. Therefore the beads have to be approached to a minimal distance given by the length of the linking molecule. The total potential for the beads is to first approximation given by the sum of their corresponding traps – the longitudinal and the transverse trap – which define a new double-well potential. Here, optical binding effects that may cause additional repulsion or attraction are ignored [S]. To estimate the minimal distance, the barrier height was calculated for the fixed parameters $F_{r/l}^{sca}(0)=0.5\,pN$, α=5 cm^{-1} and $w_0=3\,\mu m$ while varying the separation *s* of the traps and the depth U_0 of the transverse trap. As can be seen in Figure S7, the closest distance s_{min} to fulfill the 1 kT barrier condition occurs for the given operating parameters at 7.4 μm with $U_0\approx 3.8\,kT$. Smaller separation distances can be achieved if the trapping powers are increased or the potential gradients are steepend by local loss engineering. The particles can finally be made to collaps if one of the traps is turned off.

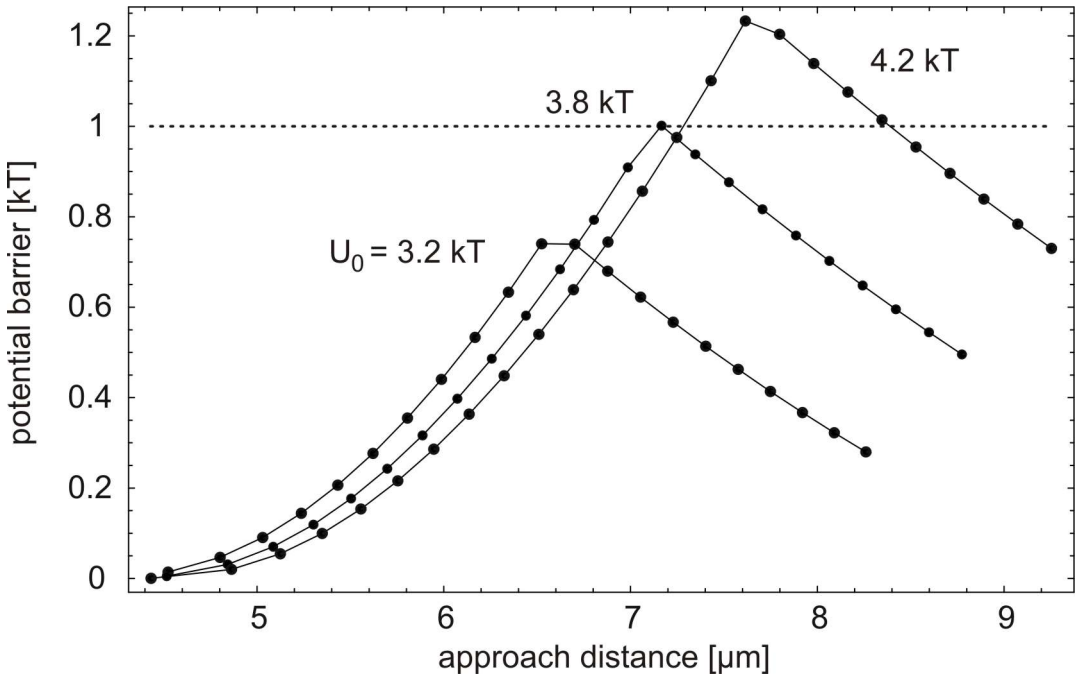

Fig. S7. Approach distance as the distance between the potential minima for two beads trapped in a transverse and longitudinal trap and the corresponding barrier height.

References

[S1] Measor, P. *et al.* Hollow-core waveguide characterization by optically induced particle transport *Opt. Lett.* **33**, 672 (2008).

[S2] Florin, E.-L., Pralle, A., Stelzer, E. & Hörber, J. Photonic force microscope calibration by thermal noise analysis *Journal Applied Physics A: Materials Science & Processing* **66** (1998).

[S3] Malagnino, N., Pesce, G., Sasso, A. & Arimondo, E. Measurements of trapping efficiency and stiffness in optical tweezers *Optics Communications* **214**, 15 (2002).

[S4] Land, D. V., Levick, A. P. & Hand, J. W. The use of the Allan deviation for the measurement of the noise and drift performance of microwave radiometers *Measurement Science and Technology* **18**, 1917 (2007).

[S5] Karasek, V. & Zemanek, P. Analytical description of longitudinal optical binding of two spherical nanoparticles *Journal of Optics A: Pure and Applied Optics* **9**, S215 (2007).